Infrared Spectra and Density Functional Calculations of MO_2, MO_3, $(O_2)MO_2$, MO_4, MO_2^- (M = Re, Ru, Os) and ReO_3^-, ReO_4^- in Solid Neon and Argon†

Mingfei Zhou,‡ Angelo Citra, Binyong Liang, and Lester Andrews*

Department of Chemistry, University of Virginia, Charlottesville, Virginia 22901

Received: August 25, 1999; In Final Form: December 13, 1999

Laser-ablated rhenium, ruthenium, and osmium atoms react with O_2 in excess neon and argon during condensation to form the MO_2 dioxide molecules as major products. The MO_3 trioxides with D_{3h} symmetry, the $(O_2)MO_2$ dioxide complexes with C_{2v} symmetry, and the tetrahedral MO_4 (M = Ru, Os) molecules are formed on sample annealing. Photolysis converts the $(O_2)MO_2$ complexes to the more stable MO_4 isomers. In addition, the MO_2^- dioxide anions and ReO_3^- and ReO_4^- anions are also formed via electron capture by the neutral molecules. The metal oxide neutrals and anions were identified from oxygen-18 substitution and natural metal isotopic splittings, and from DFT calculations of isotopic frequencies. Doping with CCl_4 to serve as an electron trap gave the same neutral molecule bands and virtually eliminated the anion absorptions, which further supports the anion identifications.

Introduction

Reactions of transition metals with oxygen are important as transition metal oxides are involved in catalytic and chemisorption processes. However, there is little experimental data available for second- and third-row transition metals especially for rhenium, ruthenium, and osmium. Both rhenium and ruthenium monoxides have been studied spectroscopically in the gas phase.[1−4] Infrared spectra of ruthenium oxides RuO_x (x = 1−4) in solid argon have been observed using a sputtering source.[5,6] Ruthenium and osmium tetroxide are stable molecules based on studies in the gas phase as well as in solution and rare gas matrices.[6−13] Ab initio (MC-SCF) calculations for RuO predict a $^5\Delta$ ground state.[14] Bonding in ruthenium dioxide, trioxide, and tetroxide has also been examined by theory.[15] The rhenium tetroxide anion is isoelectronic with osmium tetroxide, and vibrational spectra of this anion with alkali metal cations have been studied in solution and matrix isolation.[16−18]

Recent investigations of laser-ablated transition metal atom reactions with small molecules have shown very rich chemistry due to the high reactivity of ablated metal atoms compared to ordinary thermal atom reactions.[19−22] Of more importance, laser ablation produces electrons as well as metal atoms, and hence anions can be formed through electron capture by neutral molecules during sample deposition. In this paper, we report infrared spectra and density functional calculations of Re, Ru, and Os oxide molecules and anions.

Experimental Section

The experiment for laser ablation and matrix isolation spectroscopy has been described in detail previously.[23] Briefly, the Nd:YAG laser fundamental (1064 nm, 10 Hz repetition rate with 10 ns pulse width) was focused on the rotating metal target (Re, Ru, Goodfellow Metals; Os, E-VAC Products). Laser-ablated metal atoms were co-deposited with oxygen (0.05−1.0%) in excess neon or argon onto a 4 or 10 K CsI cryogenic window at 2−4 mmol/h for 30 min to 1 h. Infrared spectra were recorded at 0.5, 0.25, or 0.125 cm^{-1} resolution on a Nicolet 750 spectrometer using a HgCdTe detector. Matrix samples were annealed at different temperatures, and selected samples were subjected to broadband photolysis by a medium-pressure mercury arc (Philips, 175 W) with the globe removed.

Results

Infrared spectra of laser-ablated Re, Ru, and Os atom reaction products with O_2 in neon and argon are shown in Figures 1−6, and the absorptions are listed in Tables 1−3, respectively. Absorptions common to these experiments, namely, O_3, O_4^-, O_4^+, and O_6^+ have been reported previously[24,25] and are not listed here. Spectra after annealing and broadband photolysis are also shown in the figures.

Experiments with $^{18}O_2$ samples gave the same behavior, and the isotopic frequencies are listed in Tables 1−3. Similar experiments with mixed $^{16}O_2 + {}^{18}O_2$ and $^{16}O_2 + {}^{16}O^{18}O + {}^{18}O_2$ were also done and selected spectra are shown in Figures 7−9. In addition, neon matrix experiments were done with 0.02% CCl_4 added to serve as an electron trap, and the absorptions assigned to anions were almost eliminated from the spectra of the deposited samples.[19−22]

Density functional calculations (DFT) were done on metal oxides and anions using the Gaussian 94 program[26] and the BP86 and B3LYP functionals.[27,28] The 6-31+G(d) basis set for O atom and Los Alamos ECP plus DZ for metal atoms were used.[29,30] Calculations were first done on monoxides and dioxides and dioxide anions using both BP86 and B3LYP functionals, and the results are listed in Tables 4 and 5. Calculations were also done for MO_3, MO_4, and their anions using the BP86 functional, and the results are listed in Tables 6 and 7, respectively.

Discussion

MO. The ReO molecule has been characterized spectroscopically in the gas phase,[3,4] and the Re−O vibrational fundamental was reported at 979.1 cm^{-1} for ^{187}ReO. No absorption can be assigned to the ReO molecule in our argon and neon matrix

† Part of the special issue "Marilyn Jacox Festschrift".

‡ Permanent address: Laser Chemistry Institute, Fudan University, Shanghai, P. R. China.

* Corresponding author. E-mail: lsa@virginia.edu.

10.1021/jp993026p CCC: $19.00
Published on Web 02/08/2000

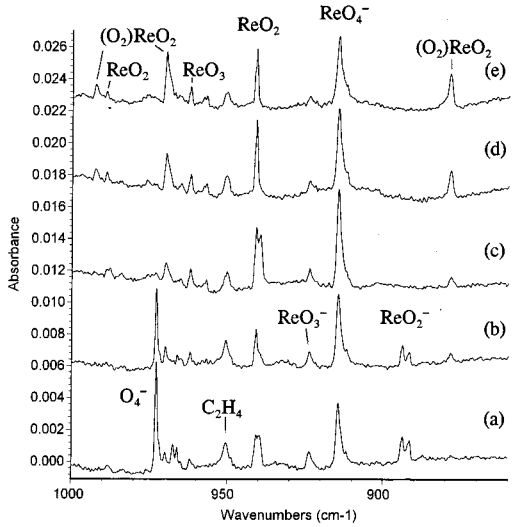

Figure 1. Infrared spectra in the 1000−860 cm^{-1} region for laser-ablated rhenium atoms co-deposited with 0.2% O_2 in neon: (a) after 30 min sample deposition at 4 K, (b) after annealing to 8K, (c) after 15 min full arc photolysis, (d) after annealing to 10K, and (e) after annealing to 12K.

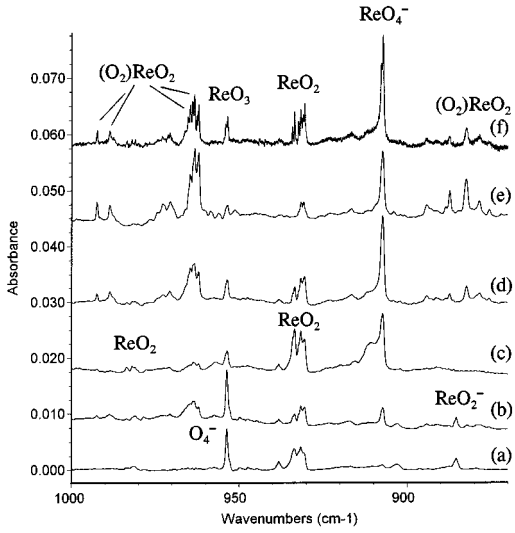

Figure 2. Infrared spectra in the 1000−870 cm^{-1} region for laser-ablated rhenium atoms co-deposited with 0.25% O_2 in argon: (a) after 1 h sample deposition at 10 K, (b) after annealing to 25 K, (c) after 15 min full arc photolysis, (d) after annealing to 30K, (e) after annealing to 35 K, and (f) 0.125 cm^{-1} resolution recorded after 30 K annealing.

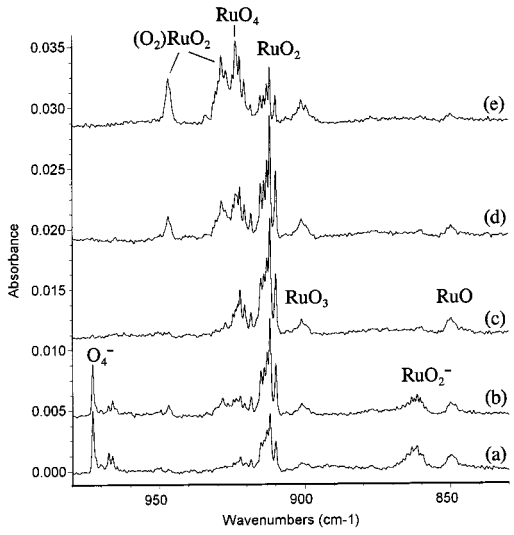

Figure 3. Infrared spectra in the 980−830 cm^{-1} region for laser-ablated ruthenium atoms co-deposited with 0.2% O_2 in neon: (a) after 30 min sample deposition at 4 K, (b) after annealing to 8 K, (c) after 15 min full arc photolysis, (d) after annealing to 10 K, and (e) after annealing to 12 K.

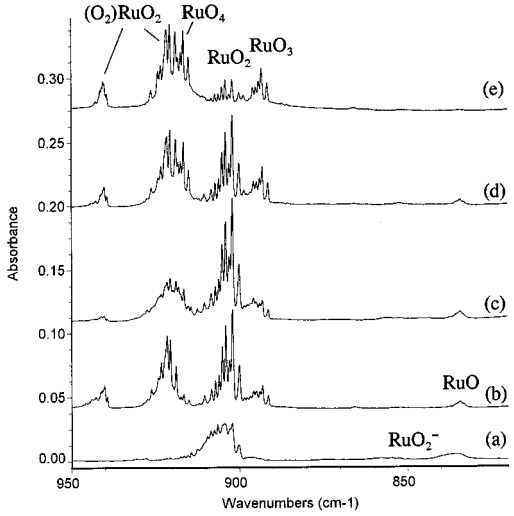

Figure 4. Infrared spectra in the 950−820 cm^{-1} region for laser-ablated ruthenium atoms co-deposited with 0.5% O_2 in argon: (a) after 1 h sample deposition at 10 K, (b) after annealing to 25 K, (c) after 15 min full arc photolysis, (d) after annealing to 30 K, and (e) after annealing to 35 K.

experiments. Both BP86 and B3LYP calculations predicted a $^4\Phi$ ground state with $^2\Delta$ and $^6\Sigma^+$ states lying slightly higher in energy for the ReO molecule. The vibrational frequency was calculated at 1014.6 (BP86) and 1029.5 cm^{-1} (B3LYP) for $^4\Phi$ ground state ^{187}ReO, which are in good agreement with the gas phase experimental value (0.965 and 0.951 scale factors).[3]

The absorption at 834.2 cm^{-1} in Ru + O_2/Ar experiments (Figure 4) is assigned to the RuO molecule. This absorption shifts to 793.4 cm^{-1} using the $^{18}O_2$ sample; the isotopic 16/18 ratio (1.0514) is just below the harmonic RuO ratio (1.0518). Although the Ru isotopic splittings are not resolved, the band shape shows the characteristic intensity pattern reflecting the natural isotopic abundance of Ru for one metal atom.[31] In the mixed $^{16}O_2$ + $^{16}O^{18}O$ + $^{18}O_2$ experiment, only a doublet is present, which confirms that one O atom is involved. This RuO assignment is in good agreement with the 834.4 cm^{-1} argon matrix value reported earlier.[5] The relative intensities of RuO and RuO_2 absorptions *reverse* in a similar experiment with the N_2O precursor. The RuO molecule is observed at 849.7 cm^{-1} in neon, blue-shifted 15.5 cm^{-1} from the argon matrix value. Both BP86 and B3LYP calculations predict a $^5\Delta$ ground state for RuO with vibrational frequency at 859.9 (BP86) and 862.7 cm^{-1} (B3LYP), and a previous MC-SCF calculation also finds a $^5\Delta$ ground state for the RuO molecule.[14]

No absorption can be assigned to the OsO molecule. Our DFT investigation finds $^5\Sigma^+$ and $^3\Phi$ states that are very close in energy; the $^3\Phi$ state is about 1.4 kcal/mol lower in energy than the $^5\Sigma^+$ state using BP86 functional, while the $^5\Sigma^+$ state is 2.7 kcal/mol lower using B3LYP. The vibrational frequency of the $^5\Sigma^+$ state is calculated at 942.4 (BP86) and 961.5 cm^{-1} (B3LYP), while the vibrational frequency of the $^3\Phi$ state is predicted at 1038.2 (BP86) and 1058.0 cm^{-1} (B3LYP).

MO_2. The absorption observed at 940.9 cm^{-1} in Re + O_2/Ne experiments decreased on annealing, but increased on broadband photolysis. In the 0.125 cm^{-1} resolution spectrum,

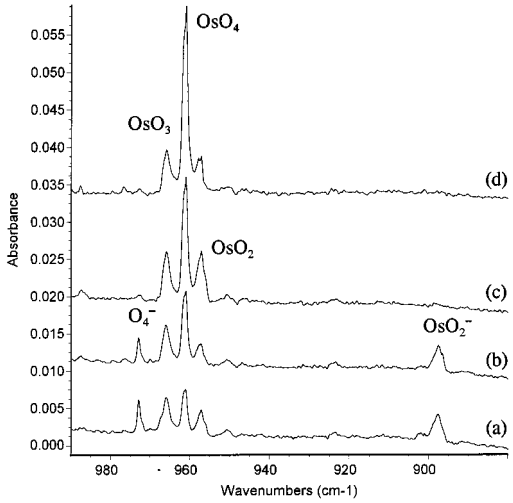

Figure 5. Infrared spectra in the 990−880 cm^{-1} region for laser-ablated osmium atoms co-deposited with 0.2% O_2 in neon: (a) after 30 min sample deposition at 4 K, (b) after annealing to 8 K, (c) after 15 min full arc photolysis, and (d) after annealing to 12 K.

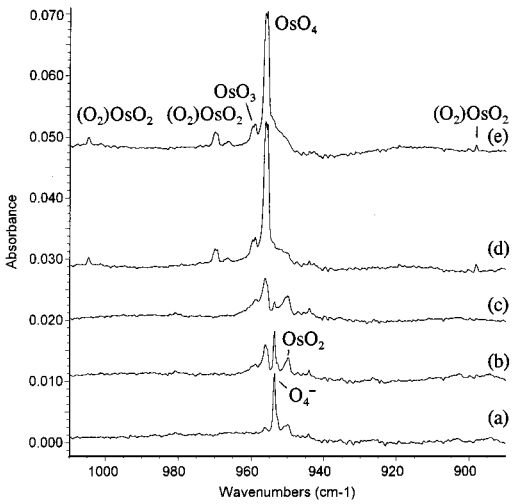

Figure 6. Infrared spectra in the 1010−890 cm^{-1} region for laser-ablated osmium atoms co-deposited with 0.5% O_2 in argon: (a) after 1 h sample deposition at 10 K, (b) after annealing to 25 K, (c) after 15 min full arc photolysis, (d) after annealing to 35 K, and (e) after annealing to 40 K.

this band resolved into two bands at 941.6 and 941.0 cm^{-1} with the relative intensities appropriate for the natural abundance of Re indicating a single Re atom vibration. These two bands shifted to 894.5 and 893.9 cm^{-1} in $^{18}O_2$ spectra, both giving a 16/18 ratio of 1.0527. In the mixed $^{16}O_2 + {}^{16}O^{18}O + {}^{18}O_2$ experiments, triplets were produced with intermediates at 906.7 and 906.2 cm^{-1}, indicating that two equivalent O atoms are involved in this vibration. These bands are assigned to antisymmetric vibrations of the $^{185}ReO_2$ and $^{187}ReO_2$ isotopic molecules. A weak band at 989.1 cm^{-1} has the same annealing and photolysis behavior, and shifted to 935.2 cm^{-1} with $^{18}O_2$ to give a 16/18 ratio of 1.0576, which is appropriate for a symmetric ReO_2 vibration. However, the Re isotopic splittings could not be resolved, as Re is less involved in this mode. The ReO_2 molecule in an argon matrix has three site splittings; the symmetric vibration was observed at 983.5, 981.9, and 981.0 cm^{-1}, and the antisymmetric vibration was observed at 934.2, 932.3, 931.0 cm^{-1} for $^{185}ReO_2$ and 933.5, 931.7, 930.5 cm^{-1} for $^{187}ReO_2$ at three different matrix sites, respectively.

TABLE 1: Infrared Absorptions (cm^{-1}) from Co-Deposition of Laser-Ablated Re with O_2 in Excess Neon and Argon

	$^{16}O_2$	$^{18}O_2$	*R*(16/18)	assignment
Ne	992.6	938.5	1.0576	$(O_2)ReO_2$, sym-OReO
	989.1	935.2	1.0576	ReO_2 ν_1
	969.8	921.1	1.0529	$(O_2)ReO_2$, asym-OReO
	962.6	914.5	1.0526	$^{185}ReO_3$
	962.0	913.9	1.0526	$^{187}ReO_3$
	941.6	894.5	1.0527	$^{185}ReO_2$ ν_3
	941.0	893.9	1.0527	$^{187}ReO_2$ ν_3
	923.7	877.9	1.0522	ReO_3^-
	914.5	868.7	1.0527	ReO_4^-
	893.8	849.5	1.0521	ReO_2^-
	891.5	847.4	1.0520	ReO_2^- site
	878.6	832.8	1.0550	$(O_2)ReO_2$, O−O
Ar	1533.1	1446.9	1.0596	$Re_x(O_2)$
	992.4	938.0	1.0580	$(O_2)ReO_2$, sym-OReO
	988.6	934.8	1.0576	site
	983.5	930.0	1.0575	ReO_2 ν_1 site
	981.9	928.3	1.0577	ReO_2 ν_1
	981.0	927.5	1.0577	ReO_2 ν_1 site
	965.3	916.8	1.0529	$(O_2)^{185}ReO_2$, asym-OReO
	964.6	916.2	1.0528	$(O_2)^{187}ReO_2$, asym-OReO
	963.9	915.3	1.0531	$(O_2)^{185}ReO_2$, asym-OReO
	963.4	914.8	1.0531	$(O_2)^{187}ReO_2$, asym-OReO
	962.7	913.7	1.0536	$(O_2)^{185}ReO_2$, asym-OReO
	962.2	913.2	1.0537	$(O_2)^{187}ReO_2$, asym-OReO
	954.0	906.5	1.0524	$^{185}ReO_3$
	953.4	905.9	1.0524	$^{187}ReO_3$
	934.2	887.6	1.0525	$^{185}ReO_2$, ν_3 site
	933.5	887.0	1.0524	$^{187}ReO_2$, ν_3 site
	932.3	886.0	1.0524	$^{185}ReO_2$, ν_3
	931.7	885.4	1.0524	$^{187}ReO_2$, ν_3
	931.0	884.6	1.0524	$^{185}ReO_2$, ν_3 site
	930.5	884.2	1.0524	$^{187}ReO_2$, ν_3 site
	907.8	862.4	1.0527	$^{185}ReO_4^-$
	907.2	861.8	1.0527	$^{187}ReO_4^-$
	887.3	840.4	1.0558	$(O_2)ReO_2$, O−O site
	885.5	841.7	1.0520	ReO_2^-
	882.4	836.3	1.0551	$(O_2)ReO_2$, O−O
	878.5	832.7	1.0550	$(O_2)ReO_2$, O−O site
	531.0	505.9	1.0496	$(O_2)ReO_2$

From rhenium and oxygen isotopic shifts for the antisymmetric stretching vibration in solid neon, the upper (oxygen isotopes) vs ^{187}Re and lower (metal isotopes) vs ^{16}O valence angle limits[32] are determined to be 130° and 124° in solid neon. We suggest a 127° ± 4° bond angle for ground state ReO_2 in solid neon.

DFT calculations predict the $^{187}ReO_2$ molecule to have a $^4B_1$ ground state with bent geometry, and antisymmetric and symmetric stretching vibrations at 945.1 and 989.8 cm^{-1} with 206:28 relative intensities using BP86 and at 973.9 and 1023.2 cm^{-1} with 260:36 relative intensities using B3LYP, which are in excellent agreement with the observed intensity ratio (approximately 7/1). The calculated ReO_2 bond angle (131.9° from BP86, 132.9° from B3LYP) is very close to the values calculated from experimental isotopic shifts.

These properties for ReO_2 may be compared to the 948.0 (ν_3), 816.4 cm^{-1} (ν_1) stretching frequencies and 140° bond angle upper limit for MnO_2 in solid argon.[33]

Bands at 918.4, 915.0, 913.9, 912.9, 911.9, and 909.9 cm^{-1} are the major product absorptions on deposition in the Ru + O_2/Ne experiments; they increased on 6 and 8 K annealing, and then decreased on 10−12 K annealing. The relative intensities match the natural isotopic abundance of ruthenium and clearly indicate the involvement of one Ru atom. The mixed $^{16}O_2 + {}^{16}O^{18}O + {}^{18}O_2$ spectra shown in Figure 7 exhibit one intermediate band centered at 876.5 cm^{-1} (partly overlapped with $^{18}O_2$ counterparts) indicating the presence of two equivalent oxygen

TABLE 2: Infrared Absorptions (cm^{-1}) from Co-Deposition of Laser-Ablated Ru with O_2 in Excess Neon and Argon

	$^{16}O_2$	$^{18}O_2$	*R*(16/18)	assignment
Ne	946.9	898.2	1.0542	$(O_2)^{102}RuO_2$, sym-ORuO
	946.1	897.3	1.0544	$(O_2)^{104}RuO_2$, sym-ORuO
	933.7	891.4	1.0475	$(O_2)^{96}RuO_2$, asym-ORuO
	931.2	889.2	1.0472	$(O_2)^{99}RuO_2$, asym-ORuO
	930.4	888.3	1.0474	$(O_2)^{100}RuO_2$, asym-ORuO
	929.4	887.4	1.0473	$(O_2)^{101}RuO_2$, asym-ORuO
	928.5	886.4	1.0475	$(O_2)^{102}RuO_2$, asym-ORuO
	926.9	884.8	1.0476	$(O_2)^{104}RuO_2$, asym-ORuO
	927.2			$^{96}RuO_4$
	924.6	882.3	1.0479	$^{99}RuO_4$
	923.7	881.3	1.0481	$^{100}RuO_4$
	923.0	880.5	1.0483	$^{101}RuO_4$
	922.2	879.6	1.0484	$^{102}RuO_4$
	920.6	878.0	1.0485	$^{104}RuO_4$
	918.4			$^{96}RuO_2$, ν_3
	915.0	875.7	1.0449	$^{99}RuO_2$, ν_3
	913.9	874.5	1.0451	$^{100}RuO_2$, ν_3
	912.9	873.4	1.0452	$^{101}RuO_2$, ν_3
	911.9	872.4	1.0453	$^{102}RuO_2$, ν_3
	909.9	870.3	1.0455	$^{104}RuO_2$, ν_3
	901.1	860.0	1.0478	$^{102}RuO_3$
	899.5	858.2	1.0481	$^{104}RuO_3$
	863.6	826.7	1.0446	$^{99}RuO_2^-$
	862.6	825.5	1.0449	$^{100}RuO_2^-$
	861.6	824.5	1.0450	$^{101}RuO_2^-$
	860.6	823.4	1.0452	$^{102}RuO_2^-$
	858.7	821.4	1.0454	$^{104}RuO_2^-$
	849.7	808.1	1.0515	RuO
Ar	942.8	894.8	1.0536	$(O_2)^{96}RuO_2$, sym-ORuO
	941.4	893.3	1.0538	$(O_2)^{99}RuO_2$, sym-ORuO
	941.0	892.8	1.0540	$(O_2)^{100}RuO_2$, sym-ORuO
	940.6	892.3	1.0541	$(O_2)^{101}RuO_2$, sym-ORuO
	940.2	891.9	1.0542	$(O_2)^{102}RuO_2$, sym-ORuO
	939.4	891.0	1.0543	$(O_2)^{104}RuO_2$, sym-ORuO
	926.2	884.9	1.0467	$(O_2)^{96}RuO_2$, asym-ORuO
	924.2	882.8	1.0469	$(O_2)^{98}RuO_2$, asym-ORuO
	923.4	881.8	1.0472	$(O_2)^{99}RuO_2$, asym-ORuO
	922.4	880.9	1.0471	$(O_2)^{100}RuO_2$, asym-ORuO
	921.6	879.9	1.0474	$(O_2)^{101}RuO_2$, asym-ORuO
	920.7	879.0	1.0474	$(O_2)^{102}RuO_2$, asym-ORuO
	918.9	877.1	1.0477	$(O_2)^{104}RuO_2$, asym-ORuO
	918.3	876.1	1.0482	$^{100}RuO_4$
	917.5	875.3	1.0482	$^{101}RuO_4$
	916.6	874.4	1.0483	$^{102}RuO_4$
	915.1	872.8	1.0485	$^{104}RuO_4$
	905.1	865.9	1.0453	$^{99}RuO_2$, ν_3
	904.1	864.8	1.0454	$^{100}RuO_2$, ν_3
	903.0	863.9	1.0453	$^{101}RuO_2$, ν_3
	902.1	862.8	1.0455	$^{102}RuO_2$, ν_3
	900.0	860.8	1.0455	$^{104}RuO_2$, ν_3
	898.7	858.2	1.0472	$^{96}RuO_3$
	895.9	855.3	1.0475	$^{99}RuO_3$
	895.0	854.4	1.0475	$^{100}RuO_3$
	894.2	853.5	1.0477	$^{101}RuO_3$
	893.3	852.6	1.0477	$^{102}RuO_3$
	891.7	850.8	1.0481	$^{104}RuO_3$
	854.6			$^{99}RuO_2^-$
	853.7			$^{100}RuO_2^-$
	852.7			$^{101}RuO_2^-$
	851.8			$^{102}RuO_2^-$
	849.9			$^{104}RuO_2^-$
	834.2	793.4	1.0514	^{102}RuO
	833.2	792.3	1.0516	^{104}RuO

atoms. The 16/18 isotopic ratios are characteristic of an antisymmetric ORuO stretching vibration, and these bands are assigned to the antisymmetric vibration of the RuO_2 molecule in neon. In argon, the RuO_2 absorptions are only partly resolved due to site splitting; the major sites of $^{102}RuO_2$ and $^{104}RuO_2$ were observed at 902.1 and 900.0 cm^{-1}, which is about 9.8 cm^{-1} red-shifted compared to the neon value. The RuO_2 frequencies in argon are in excellent agreement (-0.1 cm^{-1})

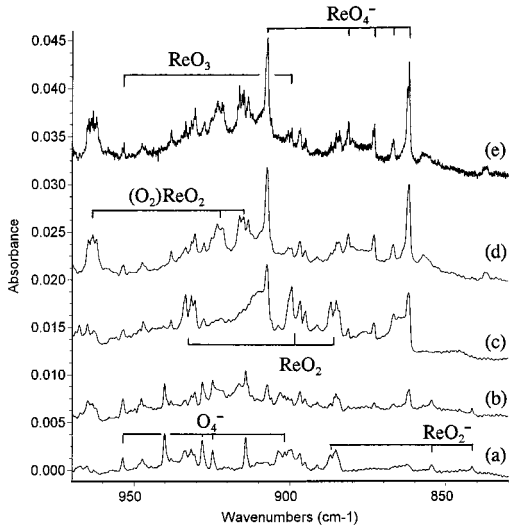

Figure 7. Infrared spectra in the 1050−830 cm^{-1} region for laser-ablated rhenium atoms co-deposited with 0.1%$^{16}O_2$ + 0.2%$^{16}O^{18}O$ + 0.1%$^{18}O_2$ in argon: (a) after 1 h sample deposition at 10 K, (b) after annealing to 25 K, (c) after 15 min full arc photolysis, (d) after annealing to 30 K, and (e) after annealing to 30 K (0.125 cm^{-1} resolution).

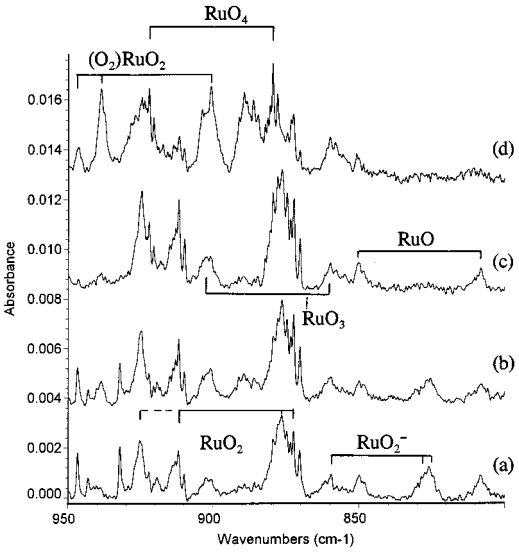

Figure 8. Infrared spectra in the 950−800 cm^{-1} region for laser-ablated ruthenium atoms co-deposited with 0.3% ($^{16}O_2$ + $^{16}O^{18}O$ + $^{18}O_2$) in neon: (a) after 1 h sample deposition at 4 K, (b) after annealing to 6 K, (c) after 15 min full arc photolysis, and (d) after annealing to 12 K.

TABLE 3: Infrared Absorptions (cm^{-1}) from Co-Deposition of Laser-Ablated Os with O_2 in Excess Neon and Argon

	$^{16}O_2$	$^{18}O_2$	*R*(16/18)	assignment
Ne	966.1	917.7	1.0527	OsO_3
	961.2	912.5	1.0534	OsO_4
	957.3	909.8	1.0522	OsO_2, ν_3
	897.5	853.7	1.0513	OsO_2^-, ν_3
Ar	1004.8	950.3	1.0574	$(O_2)OsO_2$, sym-OOsO
	970.0	921.6	1.0525	$(O_2)OsO_2$, asym-OOsO
	959.1	911.2	1.0526	OsO_3
	956.2	908.0	1.0531	OsO_4
	949.9	902.6	1.0524	OsO_2, ν_3
	898.1	848.0	1.0591	$(O_2)OsO_2$, O−O

with previous argon matrix assignments.[5] Both density functionals predict the $^1A_1$ ground state for RuO_2 with a bond angle close to 120°. The antisymmetric and symmetric stretching vibrations were calculated at 964.8 (354 km/mol)) and 947.8

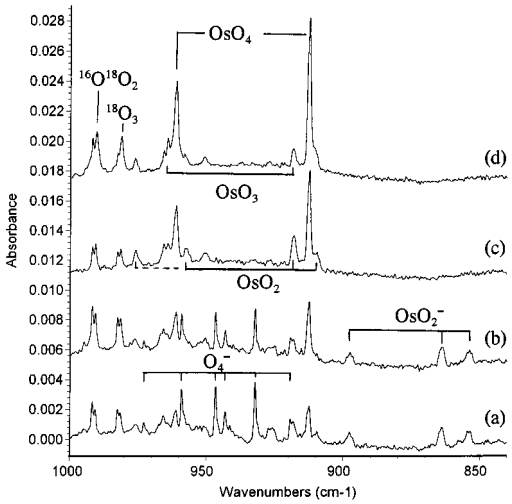

Figure 9. Infrared spectra in the 1000−840 cm^{-1} region for laser-ablated osmium atoms co-deposited with 0.3% ($^{16}O_2 + {}^{16}O^{18}O + {}^{18}O_2$) in neon: (a) after 1 h sample deposition at 4 K, (b) after annealing to 6 K, (c) after 15 min full arc photolysis, and (d) after annealing to 12 K

TABLE 4: Calculated Relative Energies (kcal/mol), Bond Lengths (Å), Vibrational Frequencies (cm^{-1}), and Intensities (km/mol) for MO Molecules (M = Ru, Os, Re)

	molecule	rel energy	bond length	freq (intensity)
BP86	RuO ($^5\Delta$)	0	1.748	859.9 (99)
	RuO ($^3\Sigma^-$)	+11.3	1.737	872.1 (65)
	OsO ($^5\Sigma^+$)	0	1.749	942.4 (46)
	OsO ($^3\Phi$)	−1.4	1.685	1038.2 (66)
	ReO ($^4\Phi$)	0	1.697	1014.6 (76)
	ReO ($^2\Delta$)	+1.5	1.639	1120.2 (73)
	ReO ($^6\Sigma^+$)	+3.9	1.752	917.0 (113)
B3LYP	RuO ($^5\Delta$)	0	1.745	862.7 (130)
	RuO ($^3\Sigma^-$)	+12.6	1.731	883.7 (74)
	OsO ($^5\Sigma^+$)	0	1.743	961.5 (57)
	OsO ($^3\Phi$)	+2.7	1.679	1058.0 (90)
	ReO ($^4\Phi$)	0	1.692	1029.5 (93)
	ReO ($^2\Delta$)	+2.2	1.632	1142.6 (104)
	ReO ($^6\Sigma^+$)	+4.8	1.749	929.0 (134)

cm^{-1} (7 km/mol) for $^{102}RuO_2$ using the BP86 functional, and 989.7 cm^{-1} (466 km/mol) and 990.1 cm^{-1} (8 km/mol) using the B3LYP functional. No symmetric vibration is observed in argon, but in the neon $^{16}O_2 + {}^{16}O^{18}O + {}^{18}O_2$ spectra, the symmetric and antisymmetric vibrations of $^{16}O^{102}Ru^{18}O$ were observed at 924.7 and 876.5 cm^{-1}, indicating that the symmetric Ru−O vibration is higher than the antisymmetric vibration, contrary to the DFT results. Apparently, the RuO_2 molecule is difficult to calculate correctly, as found for FeO_2.[34]

From isotopic frequencies for the antisymmetric vibration in solid neon, the upper and lower limits of the ORuO bond angle are estimated to be 169° and 151°, which are near the earlier argon matrix values.[5] Kay et al. also determined harmonic frquencies and calculated the true RuO_2 bond angle as 149° ± 2°, which is near the present DFT calculated values (150.1° from BP86 and 152.4° from B3LYP).

These parameters for RuO_2 may be compared with the 946 cm^{-1} antisymmetric stretching fundamental and 144° ± 5° lower bond angle limit for FeO_2.[34]

An 957.3 cm^{-1} absorption is observed in the Os + O_2/Ne experiment on deposition, with a lower relative yield in the 0.2% O_2 experiment but higher relative yield in the 0.05% O_2 experiment, suggesting that this absorption is due to an initial reaction product. The 957.3 cm^{-1} band decreased on annealing, but increased on photolysis. The $^{18}O_2$ counterpart for this band is at 909.8 cm^{-1} to give a 16/18 isotopic ratio of 1.0522, which is appropriate for the antisymmetric vibration of the OsO_2 molecule. The antisymmetric vibration of OsO_2 was observed at 949.9 cm^{-1} in argon, which is 7.4 cm^{-1} red-shifted compared to the neon matrix value. This assignment is confirmed by DFT calculations; both BP86 and B3LYP functionals predicted that OsO_2 has a $^3B_1$ ground state; the antisymmetric and symmetric stretching vibrations were calculated at 977.9 and 1011.2 cm^{-1} using the BP86 functional, while the B3LYP calculation gave 1008.3 and 1045.3 cm^{-1}, slightly higher than the BP86 values. The symmetric vibration is predicted to have only 13% of the antisymmetric vibration intensity and is not observed here. In the neon $^{16}O_2 + {}^{16}O^{18}O + {}^{18}O_2$ isotopic experiment, the intermediate band overlapped with $Os^{18}O_3$ at 917.7 cm^{-1} and gave a slightly broader band centered at 918.3 cm^{-1}. This is 15.3 cm^{-1} lower than the midpoint of the pure isotope bands, and such a highly asymmetric triplet indicates that the ν_1 and ν_3 modes are close in frequency, with the ν_1 mode slightly higher, which is exactly what the DFT calculations predict for this molecule. Although the symmetric vibrations for $Os^{16}O_2$ and $Os^{18}O_2$ were not observed, the symmetric vibration of the mixed $^{16}OOs^{18}O$ isotopic molecule was observed at 976.2 cm^{-1} in neon. From the oxygen isotopic frequencies, the bond angle upper limit is estimated to be 144° in neon and 140° in argon using the most abundant ^{192}Os isotope; hence, the true angle should be around 135°, which is in good agreement with the calculated values 131.7° (BP86) or 133.3° (B3LYP).

Two further transition metal dioxide antisymmetric stretching fundamental (ν_3) comparisons are of interest. Second- and third-row atomic sizes contrast shell expansion vs relativistic contraction,[35] which almost cancel for ZrO_2 (818 cm^{-1})/HfO_2 (814 cm^{-1}) in argon,[36] but for NbO_2 (825.9 cm^{-1})/TaO_2 (912.2 cm^{-1}) in argon,[20] MoO_2 (889.9 cm^{-1})/WO_2 (977.9 cm^{-1}) in argon, MoO_2 (901.3 cm^{-1})/WO_2 (983.9 cm^{-1}) in neon,[21] RuO_2 (902.1 cm^{-1})/OsO_2 (949.9 cm^{-1}) in argon, and RhO_2 (900.1 cm^{-1})/IrO_2 (929.0 cm^{-1}) in argon[37] pairs, the third-row oxide frequency is higher by 36.3, 88.0, 47.8, and 28.9 cm^{-1}, respectively, owing to relativistic contraction. The ν_3 frequencies increase from HfO_2 with 113° ± 5° valence angle, to TaO_2 (106° ± 5°), to WO_2 (108° ± 5°) and then decrease to ReO_2 (127° ± 3°), to OsO_2 (135° ± 5°), and to IrO_2 (linear),[37] but show a final increase to PtO_2 (linear, 961.8 cm^{-1})[38] before a decrease to AuO_2 (linear, 817.2 cm^{-1}).[39]

MO_3. Doublet bands at 954.0 and 953.4 cm^{-1} in the Re + O_2/Ar experiments increased on lower temperature annealing and then decreased on higher temperature annealing. The relative intensities of these bands match the natural isotopic abundance of Re, indicating that only one Re atom is involved in this mode. In the $^{18}O_2$ spectra these bands shift to 906.5 and 905.9 cm^{-1}, giving a 16/18 isotopic ratio of 1.0524, characteristic of an antisymmetric OReO vibration. These two bands are assigned to the doubly degenerate mode of the ReO_3 molecule which were calculated at 974.9 cm^{-1} for $^{187}ReO_3$ with C_{3v} symmetry. This mode was observed at 962.6 and 962.0 cm^{-1} in our neon matrix.

Bands at 898.7, 895.9, 895.0, 894.2, 893.3, and 891.7 cm^{-1} in the Ru + O_2/Ar experiments increased on annealing and exhibited the intensity distribution for Ru isotopes in natural abundance. The oxygen isotopic ratios (1.0472−1.0477) are appropriate for an antisymmetric ORuO vibration. These bands are assigned to isotopic RuO_3 molecules, in agreement with the previous argon matrix assignment.[5] In the neon matrix experiments, the $^{102}RuO_3$ and $^{104}RuO_3$ bands were observed at 901.1 and 899.5 cm^{-1}, blue-shifted 7.8 cm^{-1} from the argon matrix band position. Our DFT/BP86 calculation predicted the RuO_3

TABLE 5: Calculated Relative Energies (kcal/mol), Geometries, Vibrational Frequencies (cm^{-1}), and Intensities (km/mol) for MO_2 and MO_2^- (M = Ru, Os, Re) States

	molecule	rel energy	geometry M−O (Å), ∠O−M−O (deg)	ν_1	ν_2	ν_3
BP86	RuO_2 ($^1A_1$)	0	1.709, 150.1	947.8(7)	196.2(30)	964.8(354)
	RuO_2 ($^3B_1$)	+6.5	1.719, 136.3	908.2(27)	228.3(11)	942.7(196)
	RuO_2^-($^2A_1$)	−56.7	1.743, 150.7	876.8(32)	149.3(7)	893.2(464)
	OsO_2 ($^3B_1$)	0	1.712, 131.7	1011.2(20)	258.8(1)	977.9(150)
	OsO_2 ($^1A_1$)	+12.9	1.702, 122.6	1022.5(13)	298.3(2)	971.0(130)
	OsO_2^- ($^2B_1$)	−66.4	1.754, 160.2	950.0(9)	129.4(1)	924.6(395)
	ReO_2 ($^4B_1$)	0	1.726, 131.9	989.8(28)	263.5(1)	945.1(206)
	ReO_2 ($^2B_1$)	+1.4	1.699, 113.8	1025.8(25)	294.4(4)	965.6(133)
	ReO_2^- ($^3B_1$)	−59.9	1.747, 133.0	947.8(49)	233.5(1)	898.1(314)
B3LYP	RuO_2 ($^1A_1$)	0	1.697, 152.4	990.1(8)	206.1(35)	989.7(466)
	RuO_2 ($^3B_1$)	+8.3	1.708, 137.2	939.6(35)	235.1(17)	968.3(257)
	RuO_2^- ($^2A_1$)	−58.2	1.736, 155.2	900.8(32)	156.2(9)	910.2(595)
	OsO_2 ($^3B_1$)	0	1.703, 133.3	1045.3(26)	242.9(3)	1008.3(202)
	OsO_2 ($^1A_1$)	+14.5	1.692, 123.7	1058.2(20)	300.3(4)	1002.4(177)
	OsO_2^- ($^2B_1$)	−70.4	1.745, 162.5	983.5(9)	117.3(1)	954.6(472)
	ReO_2 ($^4B_1$)	0	1.717, 132.9	1023.2(36)	263.4(3)	973.9(260)
	ReO_2 ($^2B_1$)	+3.5	1.691, 115.5	1053.4(34)	278.8(7)	987.9(175)
	ReO_2^- ($^3B_1$)	−61.7	1.741, 135.6	974.7(56)	222.6(4)	923.1(384)

TABLE 6: Calculated (BP86) Geometries, Vibrational Frequencies (cm^{-1}) and Intensities (km/mol) for MO_3 (M = Ru, Os, Re) Molecules

molecule	geometry	frequency (intensity)
RuO_3($^1A_1'$)	Ru−O 1.717 Å, D_{3h}	949.7 (125), 948.0 (125), 915.8 (0), 289.8 (1), 289.7 (1), 77.5 (9)
OsO_3($^1A_1'$)	Os−O 1.713 Å, D_{3h}	1017.0 (0), 1010.0 (108), 1007.8 (117),300.6 (0.3), 299.8 (0.3), 167.6 (4)
ReO_3($^2A_1$)	Re−O 1.720 Å, ∠OReO 114.2°, C_{3v}	1004.9 (6), 975.3 (137), 974.5 (137), 314.0 (1), 313.8 (1), 205.4 (12)
ReO_3^-($^1A_1'$)	Re−O 1.745 Å, D_{3h}	962.4 (0), 933.8 (249), 932.2 (250), 291.9 (0.5), 291.2 (0.6), 149.4 (1)

TABLE 7: Calculated (BP86) Geometries, Vibrational Frequencies (cm^{-1}), and Intensities (km/mol) for MO_4 (M = Ru, Os, Re) Molecules

molecule	$^{16}O_2$	$^{18}O_2$	R(16/18)
$(O_2)ReO_2$[a] ($^2A_1$)	1010.0(72) (a_1)	955.1(68)	1.0575
	987.5(168) (b_2)	937.6(152)	1.0532
	910.6(71) (a_1)	859.6(62)	1.0593
ReO_4^-[b] ($^1A_1$)	948.5(0) (a_1)	894.2(0)	1.0607
	909.8(242) (t_2)	863.7(218)	1.0534
RuO_4[c] ($^1A_1$)	950.2(100) (t_2)	906.0(92)	1.0488
	904.0(0) (a_1)	852.2(0)	1.0608
$(O_2)RuO_2$[d] ($^1A_1$)	983.7(92) (a_1)	928.7(92)	1.0592
	956.4(177) (b_2)	912.6(162)	1.0480
	949.3(44) (a_1)	899.2(31)	1.0557
OsO_4 ($^1A_1$)[e]	976.9(0) (a_1)	920.9(0)	1.0608
	975.0(107) (t_2)	925.2(97)	1.0538
$(O_2)Os(O_2)$[f] ($^1A_1$)	1022.4(52) (a_1)	966.5(49)	1.0578
	1006.0(148) (b_2)	955.1(134)	1.0533
	953.9(64) (a_1)	899.9(55)	1.0600

[a] C_{2v} symmetry, Re−(O) 1.916 Å, O−O 1.474 Å, Re−O 1.714 Å, ∠OReO 114.2°; the Re(O_2) bisect the OReO plane. [b] T_d symmetry, Re−O 1.754 Å; the $^1A_1$ ReO_4^- is 163.8 kcal/mol lower in energy than $^2A_1$ $(O_2)ReO_2$. [c] T_d symmetry, Ru−O 1.723 Å. [d] C_{2v} symmetry, Ru−(O) 1.924 Å, O−O 1.407 Å, Ru−O 1.708 Å, ∠ORuO 121.1°; the Ru(O_2) bisect the ORuO plane; $(O_2)RuO_2$ is 27.8 kcal/mol higher in energy than $^1A_1$ RuO_4. [e] T_d symmetry, Os−O 1.727 Å. [f] C_{2v} symmetry, Os−(O) 1.919 Å, O−O 1.446 Å, Os−O 1.708 Å, ∠OOsO 117.0°; the Os(O_2) bisect the OOsO plane; $(O_2)OsO_2$ is 56.8 kcal/mol higher in energy than $^1A_1$ OsO_4.

molecule to have D_{3h} symmetry and a $^1A_1'$ ground state with antisymmetric stretching vibration at 948.9 cm^{-1} for $^{102}RuO_3$, in agreement with the first report of RuO_3.[5]

The 966.1 cm^{-1} band in the Os + O_2/Ne experiments is assigned to the OsO_3 molecule; this band increased on annealing at the expense of OsO_2. The oxygen ratio 1.0527 is appropriate for the antisymmetric OOsO stretching vibration. The counterpart in argon matrix is observed at 959.1 cm^{-1}. Our DFT calculation gave a 1008.9 cm^{-1} vibrational frequency for the $^1A_1'$ OsO_3 molecule with D_{3h} symmetry, which required a 0.958 or 0.951 scale factors to fit the experimental values in solid neon and argon.

$(O_2)MO_2$. In the rhenium argon matrix experiments, a broad band centered at 964 cm^{-1} observed only on annealing became the major absorption after higher temperature annealing. With 0.125 cm^{-1} resolution, this band resolved to three doublets, and each doublet exhibits the intensity distribution expected for rhenium isotopes in natural abundance. The oxygen isotopic ratios (1.0528−1.0537) and the rhenium isotopic splittings are appropriate for an antisymmetric OReO vibration. In the mixed $^{16}O_2$ + $^{16}O^{18}O$ + $^{18}O_2$ experiments, triplets for each band confirm that two equivalent oxygen atoms are involved in this mode. Bands at 992.4 and 988.6 cm^{-1} and 887.3, 882.4, and 878.5 cm^{-1} track with the 964 cm^{-1} band system. The 992.4 and 988.6 cm^{-1} bands give 16/18 ratios of 1.0580 and 1.0576, which are symmetric OReO vibrational ratios. The 887.3, 882.4, and 878.5 cm^{-1} bands have 16/18 isotopic ratios of 1.0558, 1.0551, and 1.0550, and rhenium isotopic splittings could not be resolved for these bands, indicating little rhenium involvement. These three band systems are assigned to antisymmetric, symmetric, and O−O stretching vibrations of the $(O_2)ReO_2$ molecule at different sites. The 531.0 cm^{-1} band is due to a Re−(O_2) stretching mode observed in this region for similar complexes.[20] These three modes were observed at 969.8, 992.6, and 878.6 cm^{-1} in solid neon. The assignments are further supported by DFT calculations, the most stable form of ReO_4 is doublet $(O_2)ReO_2$ with C_{2v} symmetry. The antisymmetric and symmetric OReO vibration and O−O stretching vibration for this species are predicted at 987.5, 1010.2, and 910.6 cm^{-1}, which are in excellent agreement with observed values; unfortunately, the mode mixing (and 16/18 ratios) of the symmetric O−Re−O and O−O stretching modes are predicted less accurately than the frequencies (scale factors 0.98, 0.98, and 0.97 for argon matrix). The O−O bond length was calculated to be 1.474 Å, in the range of 1.4−1.5 Å expected for a peroxo ligand. The O−O stretching frequency (Table 1) also falls in the range expected for a peroxo group (790−930 cm^{-1}).[40] The

$(O_2)ReO_2$ molecule is stable on photolysis, in contrast to the Ru and Os analogs.

Two sets of bands at 926.2, 924.2, 923.4, 922.4, 921.6, 920.7, and 918.9 cm^{-1} and 942.8, 941.4, 941.0, 940.6, 940.2, and 939.4 cm^{-1} in Ru + O_2/Ar experiments increased together on annealing and disappeared on photolysis when the tetrahedral RuO_4 absorptions greatly increased. Both band sets exhibit intensity distributions for natural abundance ruthenium isotopes, indicating one Ru atom involvement. The Ru and oxygen isotopic ratios for the upper and low band sets are characteristic of symmetric and antisymmetric ORuO stretching vibrations, respectively. In the mixed $^{16}O_2 + {}^{16}O^{18}O + {}^{18}O_2$ experiment, triplets were observed for both band sets which confirm that two equivalent oxygen atoms are involved in these two modes. These two band sets are assigned to the antisymmetric and symmetric ORuO stretching vibrations of the $(O_2)RuO_2$ molecule, which were observed at 946.9 and 928.5 cm^{-1} for $(O_2)^{102}RuO_2$ in solid neon, blue-shifted 6.7 and 7.8 cm^{-1} from the argon matrix values. Our DFT calculation predicted that the $^1A_1$ ground state $(O_2)RuO_2$ molecule is 27.8 kcal/mol higher in energy than tetrahedral RuO_4, but conversion of the stable complex to the tetroxide requires activation. The antisymmetric and symmetric ORuO and symmetric O−O stretching modes were calculated at 956.4, 949.3, and 983.7 cm^{-1}; the DFT vibrational frequencies do not fit as well as found for $(O_2)ReO_2$. No band can be assigned to the O−O stretching vibration; this weaker band should be sharp with little Ru involvement, so it could easily be overlapped by other bands. However, the calculation predicts an O−Ru−O angle in the $(O_2)RuO_2$ complex of 121°, and the neon matrix data provide 128° and 116° upper and lower limits. Both DFT and neon matrix isotopic ν_3 data show that the O−Ru−O angle decreases about 30° when O_2 is complexed to RuO_2.

In Os + O_2/Ar experiments, absorptions at 1004.8, 970.0, and 898.1 cm^{-1} increased together on high-temperature annealing. The 970.0 and 1004.8 cm^{-1} bands exhibited antisymmetric and symmetric OOsO stretching vibrational ratios, suggesting an OOsO subunit in this molecule. The 898.1 cm^{-1} band showed almost pure O−O stretching vibrational ratio, and these three bands are assigned to the $(O_2)OsO_2$ molecule following the $(O_2)ReO_2$ and $(O_2)RuO_2$ examples. DFT calculations predict that the $^1A_1$ ground state $(O_2)OsO_2$ is 56.8 kcal/mol higher in energy than tetrahedral OsO_4. The three vibrational modes were predicted at 1022.4, 1006.0, and 953.9 cm^{-1} (scale factors 0.98, 0.96, and 0.94) with isotopic ratios in excellent agreement with observed values, so in this case the normal modes are correctly described. The $(O_2)OsO_2$ absorptions disappeared on photolysis while the OsO_4 band appeared, which is consistent with activation to break the peroxo bond and allow formation of the more stable tetroxide molecule.

The dioxide peroxo complexes have been considered for several metals (V, Nb, Ta family; Cr, Mo, W family; Co, Rh, Ir family; and Mn, Fe, and Ni). This $(O_2)MO_2$ structure is the dominant MO_4 form for the V, Cr, and Co families, for Mn and for Fe.[20,21,33,34,36,37,41] It is therefore no surprise to find the $(O_2)MO_2$ complex for Re, Ru, and Os. Furthermore, these are the most strongly bound peroxo complexes yet characterized (DFT calculated O_2 binding energies are 82.6, 44.4, and 69.0 kcal/mol, respectively). If the dioxides ReO_2, RuO_2, and OsO_2 are considered M(IV) oxides, then the $(O_2)MO_2$ complexes are formally M(VI) oxides, as found for Rh and Ir.[37] In the nickel family, the diperoxo molecule $(O_2)Ni(O_2)$ appears to dominate, but $(O_2)NiO_2$ is also present.[42]

MO_4. RuO_4 has been studied in solid argon,[6] and a band at 916.9 cm^{-1} has been assigned to the t_2 mode of $^{102}RuO_4$ with tetrahedral symmetry. The same band observed in our Ru + O_2/Ar experiments increased on higher temperature annealing. The neon matrix counterpart is 923.0 cm^{-1}. Our DFT calculation predicted that the $^1A_1$ ground state RuO_4 with tetrahedral symmetry is the most stable isomer of RuO_4. The t_2 mode was calculated at 950.2 cm^{-1} for $^{102}RuO_4$, which requires 0.965 and 0.971 scale factors to match the argon and neon matrix values, respectively.

OsO_4 is a well-known molecule with tetrahedral symmetry.[8,10] The bands at 961.2 cm^{-1} in neon and 956.2 cm^{-1} in argon increased markedly on annealing and are assigned to the OsO_4 molecule, which are in good agreement with the 960 cm^{-1} gas phase[8] and 956 cm^{-1} argon matrix[10] values. DFT calculation predicted the t_2 and a_1 modes at 975.0 and 976.9 cm^{-1}, which are in excellent agreement with experimental values.

MO_2^-. The 893.8 and 891.5 cm^{-1} absorptions were observed on sample deposition in Re + O_2/Ne experiments, slightly decreased on annealing, and destroyed on full arc photolysis. Additional higher temperature annealing failed to reproduce these bands. Both bands were eliminated with 0.02% CCl_4 added, which strongly suggests the anion assignment.[19−22] These bands shifted to 849.5 and 847.4 cm^{-1} with $^{18}O_2$ and gave the 16/18 ratio 1.0521 and 1.0520. In the mixed $^{16}O_2 + {}^{16}O^{18}O + {}^{18}O_2$ experiment, triplets were produced with the intermediates at 862.3 and 860.4 cm^{-1}, which indicates two equivalent oxygen atoms are involved. These bands are assigned to the antisymmetric OReO stretching vibration of the ReO_2^- anion at two different sites; unfortunately, rhenium isotopes could not be resolved. The argon counterpart to these bands is observed at 885.5 cm^{-1}. DFT calculations predicted the ReO_2^- anion to have a $^3B_1$ ground state and antisymmetric and symmetric OReO stretching vibrations at 898.1 (314 km/mol) and 947.8 cm^{-1} (49 km/mol) using BP86 functional and at 923.1 (384 km/mol) and 974.7 cm^{-1} (56 km/mol), and strongly support the anion assignment. The symmetric vibrational mode was calculated to be much weaker and is not observed here. From the antisymmetric vibrational frequencies, the upper limit of the valence angle of ReO_2^- anion was calculated to be 141° in neon and 142° in argon, the true angle will be on the order of 5°−10° lower than the upper limit, and the 133.0° (BP86) and 135.6° (B3LYP) values calculated by DFT are reasonable.

In Ru + O_2/Ne experiments, a family of bands from 863.6 to 858.7 cm^{-1} observed after sample deposition decreased on annealing and disappeared on photolysis. The isotopic pattern of these bands clearly indicates the involvement of a single ruthenium atom. These bands were almost eliminated in the CCl_4 doping experiment, which supports an anion assignment. The Ru and oxygen isotopic ratios indicate that these bands are due to an antisymmetric ORuO stretching vibration; accordingly, these bands are assigned to the antisymmetric ORuO stretching vibration of the RuO_2^- anion. The upper and lower limit bond angle estimates were 180° and 163°; the true angle is probably closer to the lower limit.[5] DFT calculations predicted the RuO_2^- anion to have a bent $^2A_1$ ground state (150.7° BP86; 155.2° B3LYP); the antisymmetric and symmetric stretching vibrations of $^{102}RuO_2^-$ were calculated at 893.2 and 876.8 cm^{-1} using BP86 and at 910.2 and 900.8 cm^{-1} using B3LYP functionals, although asymmetry in the $^{16}O_2 + {}^{16}O^{18}O + {}^{18}O_2$ spectrum indicates the reverse frequency order.

The absorption at 897.5 cm^{-1} in Os + O_2/Ne experiments is assigned to the antisymmetric vibration of the OsO_2^- anion. This band, appeared on deposition, slightly decreased on annealing and disappeared on photolysis. It shifted to 853.7 cm^{-1} with $^{18}O_2$ giving the 16/18 ratio 1.0513, slightly lower than the

antisymmetric vibration of the OsO_2 molecule; this suggests a larger bond angle than found for OsO_2; a 180° upper limit is estimated for OsO_2^-, which is in line with the DFT results. The $^{16}O_2 + {}^{16}O^{18}O + {}^{18}O_2$ experiment gave a triplet with approximately 1:2:1 relative intensities. The BP86 and B3LYP calculations predicted a $^2B_1$ ground state for the OsO_2^- anion with 160.2° and 162.5° angles, respectively. The antisymmetric and symmetric vibrations were calculated at 924.6 and 950.9 cm^{-1} with 395:9 relative intensities using BP86 and at 954.6 and 983.5 cm^{-1} with 472:9 relative intensities using B3LYP.

The observed third-row transition metal dioxide anion ν_3 modes follow a trend similar to the neutral molecules but they peak at OsO_2^- rather than at WO_2^-.[20,21]

ReO_3^-. A weak band at 923.7 cm^{-1} on sample deposition in $Re + O_2$/Ne experiments decreased on annealing and shifted to 877.9 cm^{-1} with $^{18}O_2$ sample. The 16/18 ratio 1.0522 is slightly lower than the ratio for the antisymmetric vibration of ReO_2 molecule. This band was almost eliminated by CCl_4 doping, which suggests an anion assignment. Our DFT calculation predicted a $^1A_1'$ ground state ReO_3^- anion with D_{3h} symmetry and strong doubly degenerate antisymmetric OReO vibration (e mode) at 933 cm^{-1}.

ReO_4^-. The ReO_4^- anion is isoelectronic with the OsO_4 molecule, and ReO_4^- is expected to be a very stable anion like MnO_4^-. The 907.3 cm^{-1} band produced on 25 K annealing in $Re + O_2$/Ar experiments greatly increased on photolysis, and then decreased on higher temperature annealing. This band resolved into two bands at 907.8 and 907.2 cm^{-1} with relative intensities appropriate for natural abundance rhenium. The rhenium and oxygen isotopic ratios are similar to the antisymmetric OReO vibrational ratios of ReO_2, ReO_3, and ReO_2^-. In the mixed $^{16}O_2 + {}^{16}O^{18}O + {}^{18}O_2$ experiments, quintets with three weaker intermediates were observed for both bands (Figure 7); this quintet is characteristic of the triple-degenerate vibration of a tetrahedral molecule.[43] These bands were reduced by 90% with added CCl_4, again providing evidence for the anion assignment. Accordingly, the 907.8 and 907.2 cm^{-1} bands are assigned to the t_2 mode of the $^{185}ReO_4^-$ and $^{187}ReO_4^-$ anions with tetrahedral symmetry. The ReO_4^- anion was observed at 914.5 cm^{-1} in neon, blue-shifted by only 7.2 cm^{-1}. The assignment is in good agreement with the 920 cm^{-1} ReO_4^- frequency in aqueous solution.[16] Our BP86 calculation predicted a $^1A_1$ ground state for ReO_4^- with a 909.8 cm^{-1} antisymmetric vibrational frequency (t_2 mode).

Electron Affinities. There is no experimental electron affinity data for rhenium, ruthenium, and osmium oxides, and our DFT calculations provide electron affinity estimates for the neutral molecules. Similar recent calculations found that DFT predicts the electron affinities of CrO_2 and WO_2 very close (±3%) to the experimental values.[21] The ground state ReO_2^- was calculated to be 59.9 kcal/mol (BP86) and 61.7 kcal/mol (B3LYP) lower in energy than the ReO_2 neutral molecule, so 2.6 ± 0.1 eV is proposed for the electron affinity of the ReO_2 molecule. The ground state RuO_2^- anion was calculated to be 56.7 kcal/mol (BP86) or 58.2 kcal/mol (B3LYP) more stable than neutral RuO_2, and hence the electron affinity of RuO_2 is expected to be around 2.5 eV. OsO_2 has a slightly higher electron affinity than RuO_2 and ReO_2; the energy difference between OsO_2^- and OsO_2 is predicted to be 66.4 kcal/mol using BP86 and 70.4 kcal/mol using B3LYP, so the electron affinity will be near 3.0 eV. The ReO_3^- anion is calculated to be 81.8 kcal/mol lower in energy than the neutral ReO_3 molecule, the electron affinity of ReO_3 is certainly higher than for ReO_2, as full arc photolysis detached the electron from ReO_2^- but not ReO_3^-. The ReO_4^- anion absorption increased on full arc photolysis, suggesting a very high electron affinity, but there is no tetrahedral ReO_4 neutral molecule observed in the experiments. However, $(O_2)ReO_2$ is observed, and there is a huge energy difference between calculated $(O_2)ReO_2$ and ReO_4^- energies, namely 163.8 kcal/mol.

Reaction Mechanisms. The major product absorptions of laser-ablated Re, Ru and Os with O_2 in argon and neon after sample deposition are the dioxide molecules. Only the pure $M^{16}O_2$ and $M^{18}O_2$ absorptions observed in the mixed $^{16}O_2 + {}^{18}O_2$ experiments, indicating that they are formed via direct insertion reactions 1. The dioxide absorptions decreased on annealing and increased on broadband photolysis, suggesting that reaction 1 probably requires some activition energy.

$$M + O_2 \rightarrow MO_2 \ (M = Re, Ru, Os) \quad (1)$$

$$Re + O_2 \rightarrow ReO_2 \quad (1a)$$

$$Ru + O_2 \rightarrow RuO_2 \quad (1b)$$

$$Os + O_2 \rightarrow OsO_2 \quad (1c)$$

The trioxide absorptions increased on annealing at the expense of dioxide, in accord with addition reactions 2. In all of these experiments, O atoms diffuse and react, as shown by the O_3 absorption increase on annealing.

$$MO_2 + O \rightarrow MO_3 \ (M = Re, Ru, Os) \quad (2)$$

The $(O_2)ReO_2$ molecule is formed by reaction 3, which requires no activation energy, as the $(O_2)ReO_2$ absorptions increase on annealing. There are two isomers for RuO_4 and OsO_4, namely the $(O_2)MO_2$ dioxide complexes and the tetrahedral MO_4 molecules. Both increase on annealing, suggesting that they can be produced by reactions of small oxides. It appears that the $(O_2)MO_2$ molecules are formed by addition reactions 3, while the tetrahedral MO_4 molecules are produced by reactions 4. The tetrahedral molecules are more stable than the dioxide complexes based on DFT calculations. The $(O_2)MO_2$ absorptions *disappear* on broadband photolysis while the MO_4 absorptions *increase*, indicating that isomerization of $(O_2)MO_2$ to the more stable MO_4 requires some excitation to break the peroxo O−O bond. Reactions 3 are calculated by DFT to be exothermic, −82.6, −44.4, and −69.0 kcal/mol, respectively.

$$MO_2 + O_2 \rightarrow (O_2)MO_2 \ (M = Re, Ru, Os) \quad (3)$$

$$MO_3 + O \rightarrow MO_4 \ (M = Ru, Os) \quad (4)$$

$$(O_2)MO_2 + h\nu \rightarrow MO_4 \ (M = Ru, Os) \quad (5)$$

The dioxide anions are formed by electron capture of the neutral molecules, reaction 6, as are the O_3^- and O_4^- anions. ReO_3^- is probably made by electron capture, reaction 7. The ReO_4^- anions are likely formed by reaction of ReO_2^- with O_2 as the ReO_4^- absorption increases on annealing while ReO_2^- anion decreases, reaction 8. Broadband photolysis destroys the ReO_2^- and O_4^- anions and markedly increases the ReO_4^- anion absorption, suggesting that ReO_4^- anion can also be formed via electron capture by the $(O_2)ReO_2$ molecule, reaction 9.

$$MO_2 + e^- \rightarrow MO_2^- \quad (6)$$

$$ReO_3 + e^- \rightarrow ReO_3^- \quad (7)$$

$$ReO_2^- + O_2 \rightarrow ReO_4^- \quad (8)$$

$$(O_2)ReO_2 + e^- \rightarrow ReO_4^- \quad (9)$$

Conclusions

Laser-ablated rhenium, ruthenium, and osmium atoms react with O_2 in excess neon and argon during condensation to form the MO_2 dioxide molecules as major products. The MO_3 trioxides with D_{3h} or C_{3v} symmetry, the $(O_2)MO_2$ dioxide complexes with C_{2v} symmetry, and the tetrahedral MO_4 (M = Ru, Os) molecules are produced by further reactions on sample annealing. In addition, the MO_2^- dioxide anions, ReO_3^- and ReO_4^- anions are also formed via electron capture by the neutral molecules and complexes. The good agreement with frequencies and isotopic frequency ratios from density functional calculations further supports the vibrational assignments. Doping with CCl_4 to serve as an electron trap gave the same neutral molecules and virtually eliminated the anion absorptions, which adds further support for the anion identification.[19−22]

On the basis of the antisymmetric OMO vibrational frequencies for the MO_2 neutrals and MO_2^- anions, the metal dioxide neutral and anion valence angles are estimated to be 127° ± 4° for ReO_2, 151° ± 5° for RuO_2, and 135° ± 4° for OsO_2 molecules, and 135° ± 6° for ReO_2^-, respectively, which are in reasonable agreement with DFT calculated values. The RuO_2^- and OsO_2^- anions have near linear structures according to DFT calculations, which is approaching the linear structures found for the isoelectronic ORhO and OIrO molecules.[37]

Density functional calculations using the BP86 and B3LYP functionals provide electron affinities of the neutral molecules. From the calculated energy difference between neutral and anion, the electron affinities of ReO_2, RuO_2, and OsO_2 are predicted to be 2.6, 2.5, and 3.0 eV.

Now that third-row transition metal dioxide molecules have been observed for HfO_2 to PtO_2, and AuO_2, several trends can be considered.[36−39] The valence angles increase from 113° ± 5° (HfO_2) to 180° (IrO_2 and PtO_2), which is essentially the same relationship found in the first- and second-row dioxides. The third-row dioxide antisymmtric stretching frequencies for TaO_2, WO_2, OsO_2, and IrO_2 exceed the corresponding second-row fundamentals[20,21] by 29−88 cm^{-1} as a consequence of relativistic contraction.[35] The third-row dioxide antisymmetric stretching fundamentals in argon increase from 814 cm^{-1} (HfO_2) to 912 cm^{-1} (TaO_2), to 978 cm^{-1} (WO_2), and then decrease to 932 cm^{-1} (ReO_2), to 950 cm^{-1} (OsO_2), 929 cm^{-1} (IrO_2), 961 cm^{-1} (PtO_2), and 817 cm^{-1} (AuO_2), all characteristic of stable molecules with strong metal−oxide bonds.

Strongly bound peroxo complexes $(O_2)MO_2$ were observed for Re, Ru, and Os. The VI oxidation state is important[44,45] for Ru and Os and these $(O_2)MO_2$ molecules are formed spontaneously on annealing in solid argon from the O_2 and MO_2 reagents. Upon photoactivation, $(O_2)RuO_2$ and $(O_2)OsO_4$ rearranged to the more stable known RuO_4 and OsO_4 molecules.

Finally, the argon-to-neon matrix shifts observed here, 7−15 cm^{-1}, are typical of other molecules,[46] and show that these heavy metal oxides do not interact particularly strongly with the matrix.

Acknowledgment. We gratefully acknowledge NSF support for this research under grant CHE 97-00116.

References and Notes

(1) Raziunas, V.; Macur, G.; Katz, S. *J. Chem. Phys.* **1965**, *43*, 1010.
(2) Scullman, R.; Thelin, B. *J. Mol. Spectrosc.* **1975**, *56*, 64.
(3) Balfour, W. J.; Ram, R. S. *J. Mol. Spectrosc.* **1983**, *100*, 164.
(4) Balfour, W. J.; Ram, R. S. *Can. J. Phys.* **1984**, *62*, 1524.
(5) Kay, J. G.; Green, D. W.; Duca, K.; Zimmerman, G. L. *J. Mol. Spectrosc.* **1989**, *138*, 49.
(6) Green, D. W.; Kay, J. G.; Zimmerman, G. L.; Balko, B. A. *J. Mol. Spectrosc.* **1989**, *138*, 62.
(7) McDowell, R. S.; Asprey, L. B.; Hoskins, L. C. *J. Chem. Phys.* **1972**, *56*, 5712.
(8) McDowell, R. S.; Goldblatt, M. *Inorg. Chem.* **1971**, *10*, 625.
(9) Koeniger, F.; Mueller, A. *J. Mol. Spectrosc.* **1977**, *65*, 339.
(10) Beattie, I. R.; Blayden, H. E.; Crocombe, R. A.; Jones, P. J.; Ogden, J. S. *J. Raman Spectrosc.* **1976**, *4*, 313.
(11) Levason, W.; Ogden, J. S.; Rest, A. J.; Turff, J. W. *J. Chem. Soc., Dalton Trans.* **1982**, *9*, 1877.
(12) Holland, R.; Maier, W. B.; Freund, S. M.; Beattie, W. H. *J. Chem. Phys.* **1983**, *78*, 6405.
(13) Grinter, R.; Zimmerman, R. L.; Dunn, J. M. *J. Mol. Spectrosc.* **1984**, *107*, 12.
(14) Krauss, M.; Stevens, W. J. *J. Chem. Phys.* **1985**, *82*, 5584.
(15) Siegbahn, P. E. M. *J. Phys. Chem.* **1993**, *97*, 9096.
(16) Weinstock, N.; Schulze, H.; Muller, A. *J. Chem. Phys.* **1973**, *59*, 5063.
(17) Arthers, S. A.; Beattie, I. R.; Somme, R. A.; Jones, P. J.; Ogden, J. S. *J. Chem. Soc., Dalton Trans*. **1983**, 1461.
(18) Bencivenni, L.; Nagarathna, H. M.; Gingerich, K. A.; Teghil, R. *J. Chem. Phys.* **1984**, *81*, 3415.
(19) Zhou, M. F.; Chertihin, G. V.; Andrews, L. *J. Chem. Phys.* **1998**, *109*, 10893, Zhou, M. F.; Andrews, L. *J. Chem. Phys.* **1999**, *110*, 10370 (FeCO).
(20) Zhou, M. F.; Andrews, L. *J. Phys. Chem.* A **1998**, *102*, 8251 (NbO_2, TaO_2).
(21) Zhou, M. F.; Andrews, L. *J. Chem. Phys.* **1999**, *111*, 4230 (CrO_2^-, MoO_2^-, WO_2^-).
(22) Zhou, M. F.; Andrews, L. *J. Am. Chem. Soc.* **1998**, *120*, 11499 (NiCO).
(23) Burkholder, T. R.; Andrews, L. *J. Chem. Phys.* **1991**, *95*, 8697.
(24) Jacox, M. E.; Thompson, W. E. *J. Chem. Phys.* **1994**, *100*, 750. Thompson, W. E.; Jacox, M. E. *J. Chem. Phys.* **1989**, *91*, 3826.
(25) Zhou, M. F.; Hacaloglu, J.; Andrews, L. *J. Chem. Phys.* **1999**, *110*, 9450.
(26) Frisch, M. J.; Trucks, G. W.; Schlegel, H. B.; Gill, P. M. W.; Johnson, B. G.; Robb, M. A.; Cheeseman, J. R.; Keith, T.; Petersson, G. A.; Montgomery, J. A.; Raghavachari, K.; Al-Laham, M. A.; Zakrzewski, V. G.; Ortiz, J. V.; Foresman, J. B.; Cioslowski, J.; Stefanov, B. B.; Nanayakkara, A.; Challacombe, M.; Peng, C. Y.; Ayala, P. Y.; Chen, W.; Wong, M. W.; Andres, J. L.; Replogle, E. S.; Gomperts, R.; Martin, R. L.; Fox, D. J.; Binkley, J. S.; Defrees, D. J.; Baker, J.; Stewart, J. P.; Head-Gordon, M.; Gonzalez, C.; Pople, J. A. *Gaussian 94*, Revision B.1; Gaussian, Inc.: Pittsburgh, PA, 1995.
(27) Perdew, J. P.; *Phys. Rev. B* **1986**, 33, 8822. Becke, A. D. *J. Chem. Phys.* **1993**, *98*, 5648.
(28) Lee, C.; Yang, E.; Parr, R. G. *Phys. Rev. B* **1988**, *37*, 785.
(29) McLean, A. D.; Chandler, G. S. *J. Chem. Phys.* **1980**, *72*, 5639. Hrishnan, R.; Binkley, J. S.; Seeger, R.; Pople, J. A. *J. Chem. Phys.* **1980**, *72*, 650.
(30) Hay, P. J.; Wadt, W. R. *J. Chem. Phys.* **1985**, *82*, 299.
(31) *CRC Handbook*; Chemical Rubber Publishing Co., Boca Raton, FL, 1985.
(32) Allavena, M.; Rysnik, R.; White, D.; Calder, V.; Mann, D. E. *J. Chem. Phys.* **1969**, *50*, 3399. Green, D. W.; Ervin, K. M. *J. Mol. Spectrosc.* **1981**, *88*, 51.
(33) Chertihin, G. V.; Andrews, L. *J. Phys. Chem. A* **1997**, *101*, 8547 (MnO_2).
(34) Chertihin, G. V.; Saffel, W.; Yustein, J. T.; Andrews, L.; Neurock, M.; Ricca, A.; Bauschlicher, C. W., Jr. *J. Phys. Chem.* **1996**, *100*, 5261 (FeO_2).
(35) Pyykko, P. *Chem. Rev.* **1988**, *88*, 563.
(36) Chertihin, G. V.; Andrews, L. *J. Phys. Chem.* **1995**, *99*, 6356 (HfO_2).
(37) Citra, A.; Andrews, L. *J. Phys. Chem. A* **1999**, *103*, 4845 (RhO_2); **1999**, *103*, 4182 (IrO_2).
(38) Bare, W. D.; Citra, Citra; Chertihin, G. V.; Andrews, L. *J. Phys. Chem. A* **1999**, *103*, 5456 (PtO_2).
(39) Citra, A.; Andrews, L. *Theochem* **1999**, *489*, 95(AuO_2).
(40) Cotton, F. A.; Wilkinson, G. *Advanced Inorganic Chemistry*, 5th ed.; Wiley: New York, 1988.
(41) Chertihin, G. V.; Bare, W. D.; Andrews, L. *J. Phys. Chem. A* **1997**, *101*, 5090 (VO_2).
(42) Citra, A.; Chertihin, G. V.; Andrews, L.; Neurock, M. *J. Phys. Chem. A* **1997**, *101*, 3109 (NiO_2).
(43) Darling, J. H.; Ogden, J. S. *J. Chem. Soc., Dalton Trans.* **1972**, 2496.
(44) Gulliver, D. J.; Levason, W. *Coord. Chem. Rev.* **1982**, *46*, 1.
(45) Holm, R. H. *Chem. Rev.* **1987**, *87*, 1401.
(46) Jacox, M. E. *Chem. Phys.* **1994**, *189*, 144.